Bio-coated surfaces with micro-roughness and micro-porosity: Next generation coatings for enhanced energy efficiency

Soroush Niazi [1,2], *Abdolali K Sadaghiani* [1,2,*] *Ghazaleh Gharib* [1,2], *Veysel Ogulcan Kaya* [1,2], *Süleyman Çelik* [1], *Özlem Kutlu* [1,2], *Ali Koşar* [1,2,3,*]

[1]Sabanci University Nanotechnology Research and Application Center, 34956 Tuzla, Istanbul, Turkey

[2]Faculty of Engineering and Natural Science, Sabanci University, 34956 Tuzla, Istanbul, Turkey

[3]Center of Excellence for Functional Surfaces and Interfaces for Nano-Diagnostics (EFSUN), Sabanci University, Orhanli, 34956, Tuzla, Istanbul, Turkey

[*] Corresponding authors; E-mail: kosara@sabanciuniv.edu, abdolali@sabanciuniv.edu

ABSTRACT: Due to growing cooling demands as well as emerging global warming and climate change issues, cooling systems should be more efficiently utilized. Boiling is an effective heat transfer mechanism, which has a critical role in many cooling systems. Surface modification is considered as the major approach for boiling heat transfer enhancement. In this study, we developed a microbial bio-coating surface modification technique for phase change cooling applications. Thermoacidophilic *Sulfolobus solfataricus* coating was implemented using a facile dip coating method on different metallic and non-metallic surfaces. Controlled by drying conditions, the coating exhibited rough and porous morphologies. When tested in a boiling heat transfer setup, bio-coated surfaces offered enhancements up to 76.3% in Critical Heat Flux (CHF). Next, a

miniature evaporator was coated and tested for real-world air-conditioning applications, and coefficient of performance (COP) enhancements up to 11% clearly revealed the potential of bio-coated surfaces for energy saving purpose and reduction in greenhouse gasses. Furthermore, coated evaporators reduced the exergy destruction rate up to 8%. This study not only offers a new type of coating morphology, but the applicability of the proposed bio-coating is also proven in a miniature air conditioning system.

Keywords: Bio-coating, Heat transfer enhancement, Environmentally friendly coatings, Electronics cooling, Air conditioning system, Energy and exergy efficiency

Graphical abstract:

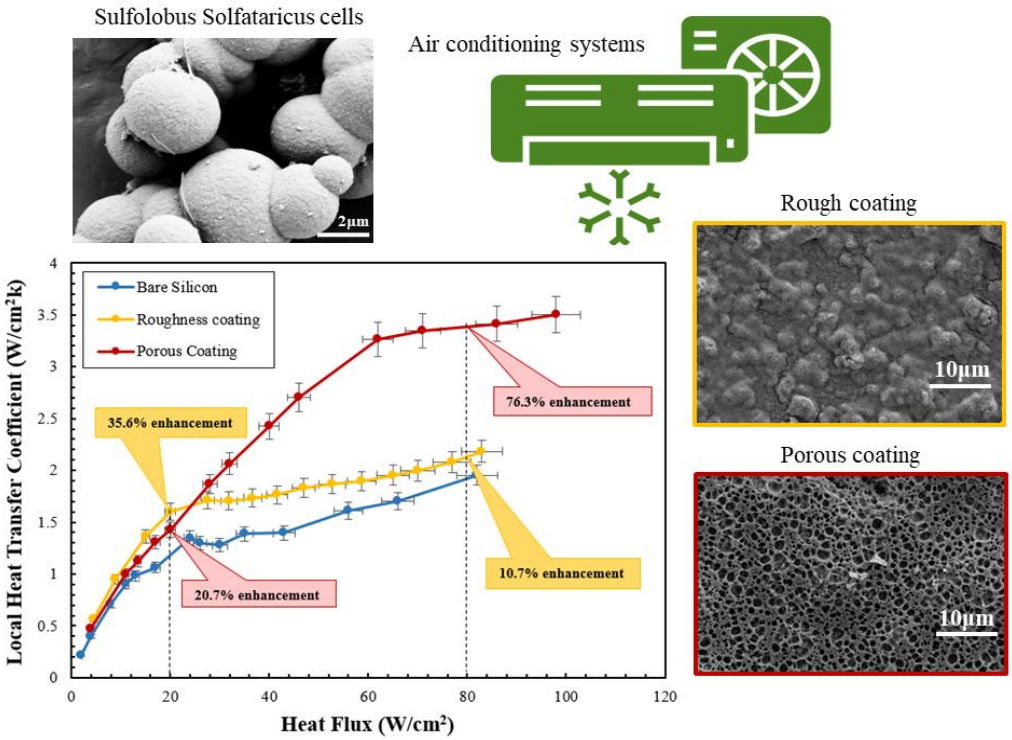

Nomenclature

Subscripts and abbreviations

AC	Air conditioning system
AFM	Atomic Force Microscopy
BHT	Boiling heat transfer
COP	Coefficient of performance
CHF	Critical heat flux
cond	Condenser
dest	Destruction
ev	Evaporator
EPS	Extracellular polymeric substance
HTC	Heat transfer coefficient
in	Inlet
ID	Inner diameter
ONB	Onset nucleate boiling
OD_{600}	Optical density at wavelength of 600 nm
OD	Outer diameter
out	Outlet
PBS	Phosphate-buffered saline
PPI	Pore number per inch
pre	Preheater
SEM	Scanning electron microscopy
WCA	Water contact angle method

Symbols

A	Heated area [m^2]
C_p	Heat Capacity [J/K]
h	Heat transfer coefficient [W/cm^2K]
h	Enthalpy [kJ/kg]
I	Current [A]
K	Thermal conductivity [K/W]
P	Pressure [KPa]
R	Thermal resistance [m^2K/W]
S	Entropy [kJ/kgK]
T	Temperature [K]
T_0	Ambient temperature [K]
T_s	Surface temperature [K]
T_{sat}	Saturation temperature [K]
V	Voltage [V]
x	Vapor quality
ΔT	Wall superheat [K]
W	Consumed work by the system [W]
Q_c	Heat by the heat source [W]
q''	Net heat flux [W/cm^2]
$\dot{m}$	Mass flow rate [kg/s]
$\dot{E}$	Exergy [W]

1. Introduction

Global warming, as a direct consequence of the increase in greenhouse gas emission, has remained the main worldwide concern during the last decades. Heat loss is the predominant form of the energy lost in energy systems/processes. One of the major sources of energy losses is linked with the constant utilization of air conditioning, refrigeration, and heat pipe systems. According to the International Energy Agency (IEA), the cooling demands in the air conditioning market is predicted to be tripled by 2050 [1]. Thus, many attempts have been made to enhance the energy

efficiency of these systems. Due to its ability to remove large quantities of heat, boiling phenomenon is used as a cooling method in air conditioning and refrigeration systems [2],[3].

Despite its superiorities compared to the conventional methods, boiling has a limit called critical heat flux (CHF), where the vapor columns create a vapor blanket film on the surface, which drastically decreases the heat transfer rate from the surface. Figure 1 shows the typical boiling regimes. At first, natural convection corresponding to single phase flow happens. The boiling process starts with the inception of bubbles from the nucleation sites on the heated surface (cavities and surface impurities). Here, the required temperature for the onset of nucleate boiling (ONB) depends on the surface morphology. As the surface temperature increases, nucleate boiling regime starts, a region characterized by more activated nucleation sites and discrete departed bubbles. Further surface temperature increment results in more generated bubbles leaving the surface in the forms of vapor columns and larger bubbles. The end of the nucleate boiling region is described by excessive generated vapor columns and blankets, which block the coolant path to the surface, thereby leading to boiling crisis or critical heat flux (CHF).

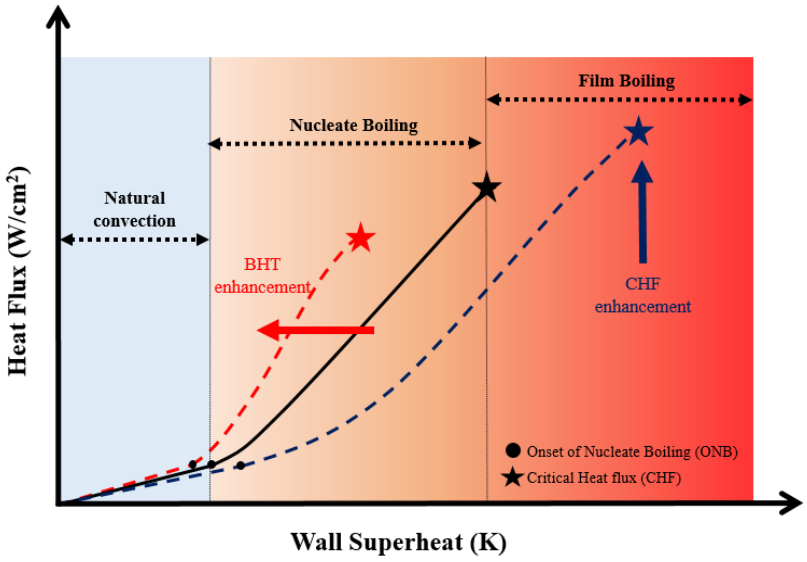

Figure 1. Boiling regimes, boiling heat transfer (BHT) and critical heat flux (CHF) enhancements in an ideal flow boiling curve.

As indicated in Figure 1, boiling heat transfer enhancement can be achieved by i) reducing ONB temperature, ii) improving heat transfer coefficient (HTC), and iii) increasing CHF [4]. Many surface modification techniques [5], [6] have been proposed and investigated to achieve these goals. These techniques include implementation of nanowire arrays [7], nanorods [8], graphene coating [9], polymer coating [10],[11], virus coating [12], biphilic surfaces [13], porous surfaces [14], laser-engineered surfaces [15], and plasma spray coating [16]. Based on the application and the range of the applied heat fluxes, these three aspects should be considered in the design of thermal-fluids systems to maximize the heat removal from the surface in nucleate boiling and film boiling regimes.

As an example for surface modification, Ma et al. [17] investigated surface area enhancement in flow boiling via micro-pin-fins. The surface revealed the effect of fin height, fluid velocity and liquid sub-cooling on heat transfer. Sadaghiani et al. [18] explored the effect of copper based micro- and nano-structured surfaces on flow boiling. Alam et al. [19] studied the effect of surface roughness on flow boiling. These studies showed that the roughness elements about the size of 1 and 1.6 μm considerably affected the nucleation site density and boiling inception. Roughness elements can majorly be introduced via mechanical modification such as sanding, etching, and deposition [6]. In the study conducted by Jung et al. [20], the effects of treated surfaces by anodization in two acids as the electrolyte (deposition) and with submicron-roughness on subcooled flow boiling of FC-72 were investigated at ambient pressure. Their observations marked an increase in HTC and CHF. Sisman et al. [21] applied roughness with the size of 1 to 4μm on aluminum sheets with mechanical sanding technique and reported that smaller roughness could create more active nucleation sites at the same heat fluxes.

In addition to roughness, tuning the porosity is one of the widely used modification techniques in boiling heat transfer. Porous foams generate a high surface area-to-volume ratio.

Rainey et al. [22] investigated the effect of micro-porosity using the ABM coating method (Aluminum particles, Devcon Brushable Ceramic epoxy, and Methyl-Ethyl-Keytone) on subcooled flow boiling of FC-72. Compared to non-coated surfaces, boiling inception took place at lower wall superheats and consequently increased heat transfer coefficients. However, the development of microporous coating using Al_2O_3 particles with size of less than 10μm resulted in 25% CHF enhancement [23]. Further investigation on R-134a flow boiling in tubes with a metallic porous surface exhibited increased heat transfer coefficient (up to 200%), as the cell size of the metal foam was changed from 20 PPI (pore number per inch) to 40 PPI [24]. In the study conducted by Pranoto and Leong [25], high thermal conductivity graphite foams with average pore diameter of 350 and 650 μm were used in flow boiling experiments. As a result, more nucleation sites on the porous surface could be observed, which raised the heat transfer coefficient by 2.5 times.

As can be seen from the abovementioned studies, the available enhancement methods require expensive infrastructure, have a complex process flow for their fabrication/preparation, and most importantly, cause environmental issues due to released hazardous materials as by-products. On the other hand, according to the latest market report published by fortune business insights, the global paints and coatings market size in 2019 was 154.6 billion USD and is expected to reach an estimated value of 249.7 billion USD in 2027 [26]. This huge budget is mostly based on the demand for new generation coatings and should be wisely managed in order to meet global energy needs. To address these issues, we used *Sulfolobus solfataricus* in this study to modify the surfaces by providing organic porous as well as roughened surfaces. Previously, this technology was formulated by our team [27]. Here, we propose the next generation bio-coating, which is highly durable, environmentally friendly, and cheap and has a practical coating method, for the implementation to thermal-fluids systems. This study not only offers new types of coating

morphologies, but also the applicability of the proposed bio-coating is proven with its implementation to a miniature air conditioning system.

2. Methods and materials

2.1. *Sulfolobus solfataricus* culture

Archaeal cells have a unicellular structure with circular chromosome. They resemble to eukaryotic cells due to their metabolisms involving DNA replication and transcription. However, they remarkably exhibit the same structure and morphology and other macromolecule metabolisms as of prokaryotes [28]. Nevertheless, archaeal domains harbor distinctive complex traits at molecular level that enable them to endure extreme physiological conditions such as low or high temperatures (−2 °C to 15 °C or 60 °C to 122 °C), high salinity (2 M to 5 M NaCl), and low or high pH (<4 or >9) [29],[30],[31]. *Sulfolobus solfataricus* is a hyperthermophilic sulfur metabolizing archaeon, which belongs to Crenarchaeota phylum. This species grows best at temperatures around 80° C and highly acidic pH (2-4). *Sulfolobus solfataricus* essentially metabolizes sulfur as a main cellular metabolism. *Sulfolobus solfataricus* cells generally have a spherical shape processing flagellums, which generate frequent lobes [32]. Highly thermostable properties of this species make it a strong candidate for biotechnological applications regarding heat transfer enhancement.

The initial batch of *Sulfolobus solfataricus* was purchased from American Type Culture Collection (ATCC® 35092™), and the growth medium was prepared according to the ATCC® Medium 1304 recipe. The medium composition is provided in Table S1. Since *Sulfolobus solfataricus* prefers anaerobic growth, the initial cultivation rate was relatively slow during the preparation. In order to reach maximum growth rate, the culture volume was stepwise increased. Conical flask containing 30mL of pre-warmed medium was first inoculated using aliquot of the cell vial. Then, the cell growth was monitored using UV Spectrophotometer at OD_{600} for 72 - 96h.

The culture volume was gradually increased up to 100 mL, 250 mL, and 500 mL by adding pre-warmed medium. To generate the mass production of the archaeon in a sustainable manner, the growth medium was supplied with 2 g/L D-sucrose, and the cells were grown at constant temperature and PH of 84°C and 3.9, respectively.

When the OD_{600} of culture reached to 1, 250 ml of the culture was harvested after cooling down on ice and further harvested using centrifugation at 4500 ×g for 15 min. The remaining culture was added with the fresh medium up to 500 ml and was kept for further incubation. Then, the supernatant was discarded, and the pellet was stored at −80 °C until use.

In order to prepare bio-coated surfaces, the pellet was washed once with 250ml of phosphate buffer (20% (v/v) in H_20) at room temperature and then re-suspended with 250ml of fresh phosphate buffer. Finally, Poly-L-lysine (0.1 % (w/v) in H_2O) was added into the suspension with a ratio of 1:5 to increase the adhesion of the biomaterial to the desired surface. Then, the coating mixture was applied on the silicon wafer with thickness of 500µm and interior side of an evaporator made of aluminum. Subsequently, the coated samples were incubated at room temperature as well as at 60°C to initiate the evaporation process. Figure S1 summarizes the culture, coating and drying processes. More information about the coating process of the aluminum tube is provided in the Supporting Information (Figure S2).

2.2. Surface characterization

Once coated surfaces were completely dried, they were processed for the surface characterization. To avoid disparity, which might generate as a result of surface charge formation of biomaterial, and to develop homogeneous surface for high resolution image processing, a thin layer (3-4 nm) of gold-palladium alloy was employed using SEM sputter coater. A scanning electron microscope (SEM Leo Supra 35VP, Oberkochen, Germany) was used to capture the microscale images of the coated samples. The Secondary Electrons (SE) mode was used for the

imaging due to its high spatial resolution. The images were taken using the SE mode at low voltage (3KV and 10KV) in 0 and 45 degree titled visions to obtain both full images of the surface area and the cross sectional area. The wettability of the bio-coated surfaces was measured using the water contact angle (WCA) method [33]. A 5μL of the water drop was applied on the five various spots of each sample, and their relevant average contact angle was determined.

Surface characterization using AFM (Atomic Force Microscopy) indicated that the average thickness in porous and roughened surfaces was 1.2 μm. The drying time of the samples incubated at room temperature was 30 hours, whereas the drying time of the specimens incubated in the oven at 60°C was 1.5 hours.

Figure 2a shows the *Sulfolobus Solfataricus* cells fixed on the substrate surface (using 2.5% glutaraldehyde dissolved in phosphate-buffered saline (PBS) and kept at the room temperature for drying). The resulting electron microscopy image of the highly diluted single cell sample that lacks fixation solution is shown in Figure 2b. This sample was dried under the freeze-drying condition for 2 hours. This figure shows that the morphology of the cell remained intact, while the interior fluid material was completely dried as a result of the ice sublimation and formed the porous structure. Figure 2c and Figure 2d demonstrate the dried bio-coating (concentrated cells with poly-l-lysine) on silicon substrates under different drying conditions.

In addition to silicon and glass surfaces, the bio-coatings were prepared and characterized on metallic surfaces including copper, aluminum and stainless-steel (Figure S3). Similar to silicon and glass substrates, metallic surfaces also have rough and porous morphologies under dip coating conditions.

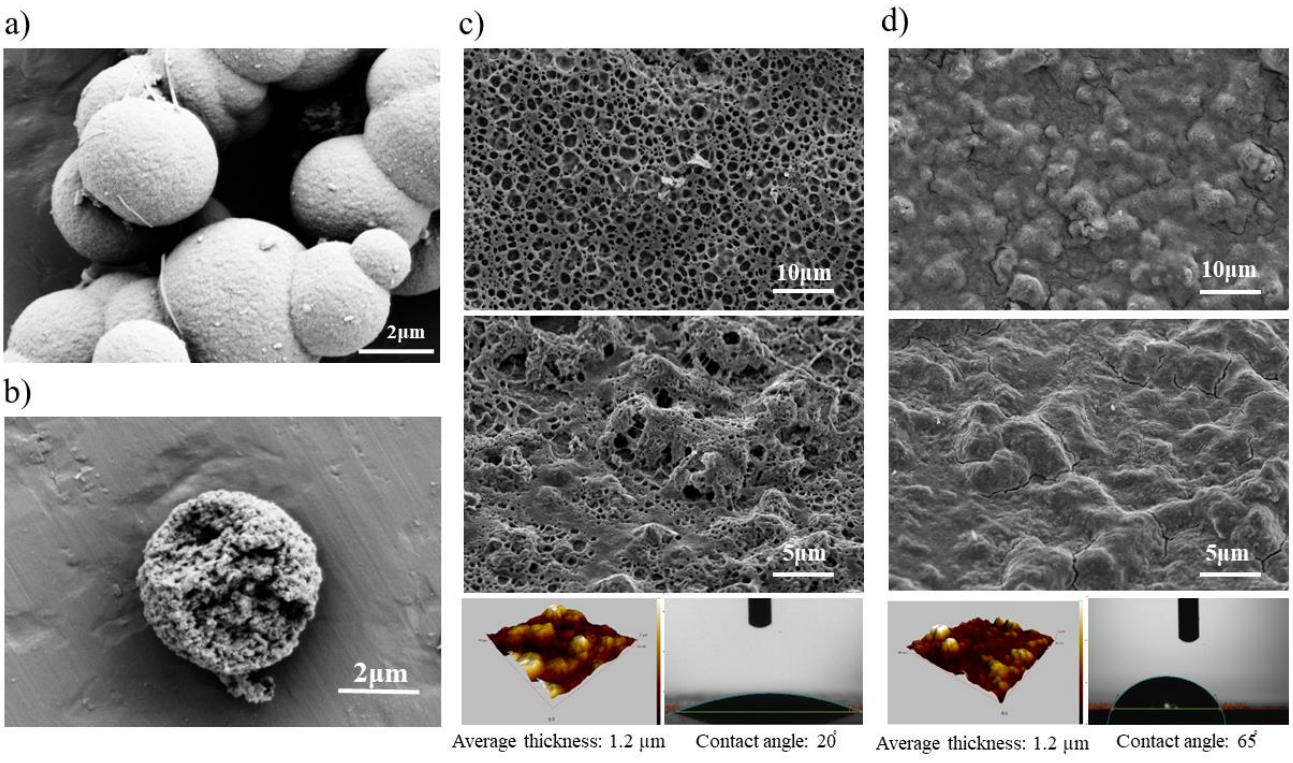

Figure 2. a) *Sulfolobus Solfataricus* fixed cells on the substrate. **b)** Single cell of *Sulfolobus Solfataricus* in a highly diluted sample and the porous structure inside the cell. 2D and 3D SEM images, AFM results and contact angles of the coated samples under two different drying conditions: **c)** Porous surface achieved at 60°C heat incubation, **d)** Roughened surface achieved after drying at room temperature.

3. Results and discussion

3.1. New surface morphology for phase change systems

The bio-coating surface is inspired by microbial biofilm formation. Generally, the biofilm formation is considered as a significant survival mechanism in microbial life, which protects the microorganism from austere conditions such as nutrient scarcity or unfavorable temperature. Similar to bacterial cells, archaeal cells form biofilm, where cells initiate the self-immobilization and build up the stacked layers to adapt to the temporary mutual lifestyle. In the biofilm process, cells inevitably produce multilayer microbial community, which leads to irreversible attachment, subsequent development of micro colonies and a further process for the biofilm maturation. In

response to various stress states, death signals induce autolysis of some microbes to provide nutrition for colony survival known as “die for community” [34].

The proposed bio-coating process employs *Sulfolobus Solfataricus* to form a biofilm on the surface using poly-l-lysine to act as an extracellular polymeric substance (EPS). The structure of the bio-coated layer developed under the room temperature displays roughness mainly due to smooth autolysis of the surface microbial biofilm. However, the porous shape structures form due to the rapid release of the gasses such as H_2S, CO_2 and SO_2, which consequently generate a distinct morphological structure on the biofilm (Figure 3). These porous structures identified as micro and nano structures reflect the trace of the released gasses and demolished cells. In addition, the rapid evaporation withdraws more dissolved gases to the bio-layer/air interface and aligns the micro-organisms in dispersed fashion and thus establishes the porous structure. On the other hand, evaporation at room temperature corresponding to the steady state form of evaporation allows micro-organisms to slowly descend on the substrate and forms the roughened coating.

Most of the Sulfolobus species display aerobic growth. However, *Sulfolobus Solfataricus* has a higher growth rate at low oxygen concentrations [35]. Aerobic microorganisms grow in the presence of the oxygen when the O is the final electron acceptor and water and CO_2 are the final products. Additionally, Sulfolobus species are known to be chemosynthesis microorganisms due to their ability in oxidizing sulfur to metabolize various carbon sources and consequently direct the energy for carbon fixation. Our carbon source to grow *Sulfolobus Solfataricus* is D-sucrose. Sucrose is a disaccharide consisting of glucose and fructose. Aerobic metabolism generates CO_2 as a result of the glucose oxidation. Basically, they gain energy from growing on sulfur or various organic compounds. Sulfur metabolism pathways in archaea are part of the food chain survival strategy, when there is a lack of energy source, sunlight, nearby hydrothermal vents, with abundant

hydrogen sulfide and carbon dioxide. The SO_4^{2-} is the prerequisite in sulfur metabolism pathway of *Sulfolobus Solfataricus,* which produces H_2S gas through three sequential reactions [36] as indicated in Figure 3. Moreover, these microorganisms could metabolize organic sulfur and emit H_2S under aerobic conditions [37]. It was reported that in some studies the rate of oxidation is determined by the biogeochemical characteristics of the sediment in sulfur-oxidizing microorganisms [38],[39]. According to these studies, the rate of the sulfur oxidation in such microbes is more on the sediment surface, where enormous amount of the oxidants is available as a result of high rate sulfur reduction [40]. Most of the sulfide oxidizing microorganisms grown in lab cultures are mostly derived from surface sediments [41].

Temperature discrepancy between two samples is the main reason to generate various morphologies defined as roughness and porous coatings. This temperature difference has two main effects on the evaporation rate and resulting cell sedimentation: i) Surface evaporation occurs as a result of vapor transport at the bio-film/air interface. The vapor transport is highly dependent on the diffusion coefficient of the dissolved gas, where the diffusion coefficient exponentially increases with the temperature [42]. For example, the diffusion coefficient of air is almost five times higher at 60°C compared to the room temperature. ii) The second reason is derived from the differences in solubility of the generated gases within the biomaterial at different temperatures. At higher temperatures, the solubility of the generated gases such as H_2S, SO_2, CO_2 and air decreases exponentially and results in major difference in gas release from the bio-film (Table 1). This rapid release of the gasses at 60°C contributes to the alteration in sedimentation profile and also the bio-film rupture.

Table 1. Solubility of the gases in water (g gas per kg water) [43]

Gases in the biomaterial	At 20°C	At 60°C	Percentage of reduction
CO_2	1.7	0.6	64.7%

H_2S	3.85	1.5	61%
SO_2	115	45	60.8%
Air	0.024	0.013	45.8%

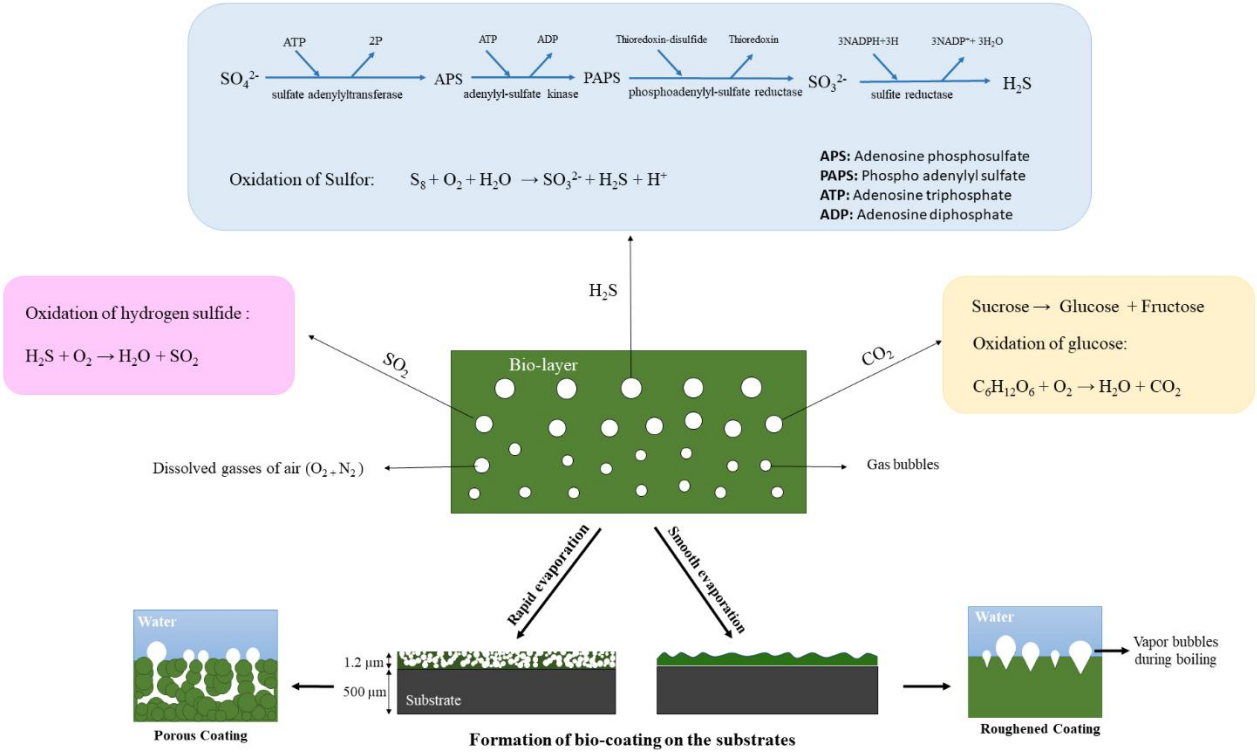

Figure 3. Generation of CO_2, H_2S and SO_2 as a result of *Sulfolobus sulfactorius* biological metabolism [36]. Figure depicting evaporation of bio-layer under two different conditions (rapid and smooth). The rapid evaporation results in formation of the porous structure, whereas smooth evaporation causes roughened bio-film on the substrate. The schematics represent two various bio-coated morphological surfaces and their function once boiling occurs.

3.2. Testing and analysis method

The bio-coated (porous- and rough-coated) surfaces were tested in a flow boiling experimental setup to investigate the effect of surface properties on boiling heat transfer and two-phase flow behavior. More information about the experimental setup and procedure can be found in Supporting Information (Figure S4). A channel with dimensions of 50×15×0.5 mm^3 and equipped with pressure and temperature sensors was used to perform flow boiling experiments.

The experiments on non-coated and bio-coated surfaces were performed under the atmospheric pressure at the mass flux of ~100 kg/m^{2}s (corresponds to average mass flux of miniature air-conditioning systems [44]). The wall superheats (ΔT_{sat}) – defined as the temperature difference between the surface (T_s) and saturation temperature (T_{sat}) – were obtained for the applied heat inputs. The comparisons of the heat transfer performance between non-coated and coated surfaces are presented in Figure 4. It should be noted that each test was repeated for three times to ensure the repeatability of the experiments. The local heat transfer coefficient is calculated as:

$$h = \frac{1}{A}\frac{Q}{\Delta T_{sat}} \tag{1}$$

In equation 1, Q is the net heat input (W), ΔT_{sat} is the wall superheat (K), and A is the surface area (m^2). Four temperature measurements were used to calculate the average temperature of the surface in the aluminum block (at 4 mm beneath the substrates). The average of the measurements was used as the surface average temperature.

$$T_{\ average} = \frac{T_1 + T_2 + T_3 + T_4}{4} \tag{2}$$

The net heat flux, heat loss, and surface temperatures are calculated using equations (3) to (5):

$$q'' = \frac{IV - Q_{Loss}}{A} \tag{3}$$

$$Q_{Loss} = IV - \dot{m}c_p\Delta T = \ Heat\ loss\ percentage\ \times\ IV \tag{4}$$

$$T_{surface} = T_{average} - q''(\frac{L_{Al}}{K_{AL}} + \frac{L_{Silicon}}{K_{Silicon}} + R_{paste}) \tag{5}$$

where I, V, and A are the applied current (A), voltage(V), and the heated area (m^2), respectively. Heat loss is the difference between input power and the amount of heating needed at a specified mass flow rate at a constant ΔT. The percentage of the heat loss in the boiling setup was calculated less than 8%. L_{Al} is the vertical length between surface temperature measurement location and

substrate, and $L_{Silicon}$ is thickness of the silicon wafer, which is 500 μm. K is the thermal conductivity, and $R_{paste} = 6 \times 10^{-6}\ \frac{m^2 k}{W}$ is the thermal resistance of the thermal paste used to reduce the thermal resistance between two surfaces.

3.3. Heat transfer performance

Figure 4a clearly reveals that the porous-coated surface has higher CHF values compared to other surfaces. Furthermore, higher CHF values were obtained at lower wall superheat, which suggests lower surface temperatures for the porous-coated samples. The main reason for enhancements is the interconnected pore networks, which enhance the liquid wetting and vapor venting at higher heat fluxes (shown in Figure 4b). Accordingly, enhancements of 11%, 20.7%, 74.5%, 94.1% and 76.3% are achieved at 10 (W/cm^2), 20 (W/cm^2), 40 (W/cm^2), 60 (W/cm^2), and 80 (W/cm^2) heat fluxes, respectively.

The obtained results for rough-coated surfaces also prove enhancements in HTC and CHF. The roughened surface provides abundant nucleation site densities, and the performance of this surface appears to be better at lower heat fluxes, while its function gradually deteriorates at higher heat fluxes. Enhancements of 22%, 35.6%, 25.7%, 15.7% and 10.7% are obtained at 10 (W/cm^2), 20 (W/cm^2), 40 (W/cm^2), 60 (W/cm^2), and 80 (W/cm^2) heat fluxes, respectively. As can be seen, compared to other samples, rough surfaces have a better cooling performance at low wall superheats (ΔT_{sat}<15K). At this range of wall superheats, the rough-coating offers smaller bubbles compared to the porous-coated surface, which is a result of abundant nucleation sites provided by this type of coating. The visualization studies at the applied heat flux of 20 W/cm^2 indicate that the bio-coated samples resulted in the formation of more bubbles and heat transfer enhancement (Figure 4b).

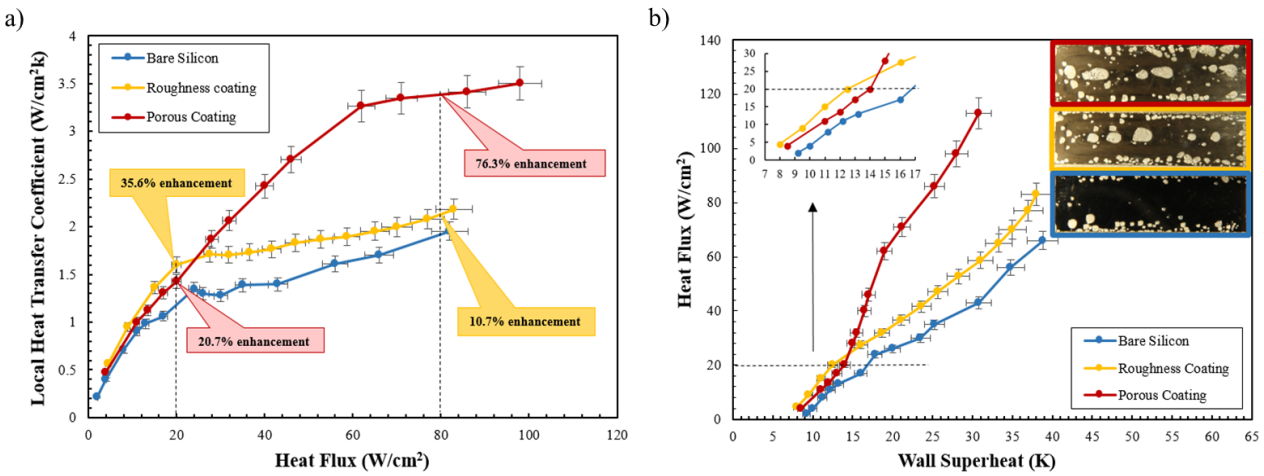

Figure 4. The effect of roughened and porous bio-coated surfaces on boiling heat transfer at the mass flux of 100 kg/m^{2}s. **a)** Local heat transfer coefficient profile and enhancements for nucleate boiling regime and near CHF, **b)** Wall superheat-heat flux profile and boiling images of the non-coated and bio-coated surfaces at nucleate boiling regime for the heat flux of 20 W/cm^2

Visualization studies were performed on the bio-coated and non-coated surfaces. The visualization results on the rough-coated clearly indicate the generation of tiny bubbles (marked in yellow in Figure 5a). This is due to presence of abundant nucleation sites on the rough-coated surfaces. However, on the non-coated surfaces, many slugs (large vapor bubbles) can be observed. These slugs prevent the surface rewetting path and results in a high surface temperature beneath the large vapor bubbles. On the other hand, on the rough-coated surface, these tiny bubbles move towards the surface, thereby rewetting the surface and increasing the cooling efficiency of the surface (marked in red in Figure 5a) [45].

On the porous-coated surfaces, as a result of the presence of many interconnected channels (as shown in SEM images in Figure 2c), transportation of coolant within the bio-coating takes place during the boiling process, especially at higher heat fluxes. These interconnected channels act as liquid supply paths when large vapor blankets form at high temperatures. As a result of this effect, the flow morphology (distribution of vapor phase inside the two-phase flow) changes dramatically.

As can be seen in Figure 5b, compared to the non-coated surface, the porous-coated surface houses a more distributed vapor phase, which is more evident at high heat fluxes ($q \geq 40$ W/cm^2).

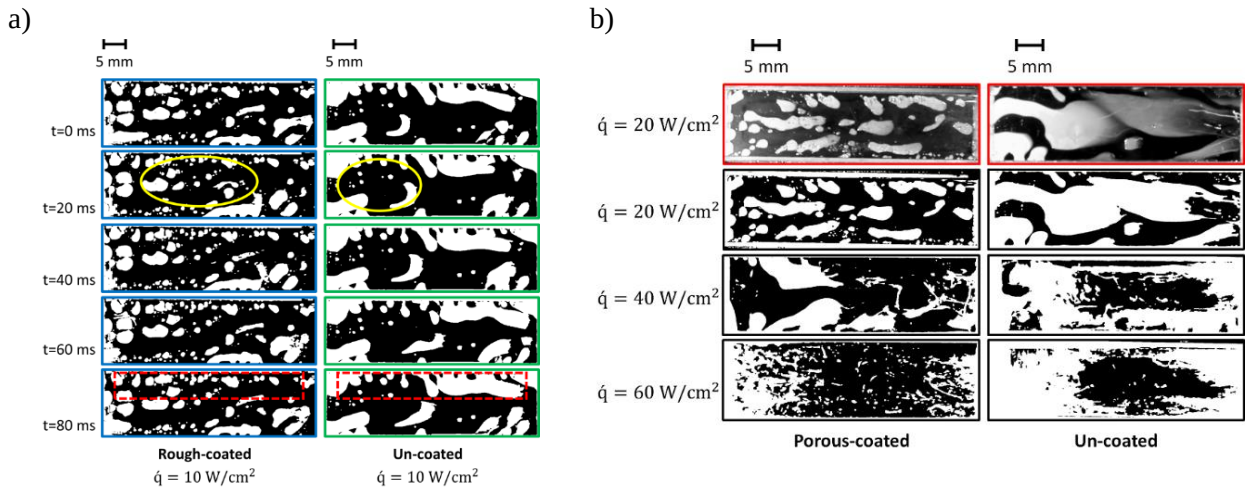

Figure 5. Images captured boiling experiments. a) Rough-coated surface at constant heat flux, b) porous-coated at different heat fluxes. Here, liquid and vapor phases are shown in black and white colors, respectively.

3.4. System performance analysis

Based on the obtained promising results from the boiling experiments, a miniature air conditioning system was assembled to examine the performance of the bio-coated evaporators. First and second laws of thermodynamic are used to analyze the performance of the system. In the energy analysis, when the first law of thermodynamics is considered, all types of energy are taken into account and the quality of energy types is neglected. For instance, it is not possible to show the change in the quality of thermal energy from the hot ambient air (heat source) to the evaporator surface (cold source). On the other hand, the exergy analysis involving the second law of thermodynamics leads to a better understanding about the energy transfer process. Basically, the exergy of the system represents the maximum amount of the work when the system comes back to its equilibrium with the environment. This is especially important for cooling applications, where the system will have a waiting period for the next cooling cycle.

3.4.1 Energy analysis, first law analysis

Figure 6a shows the schematic of the lab-made closed-loop system. Detailed information about the experimental setup is provided in Supporting Information (Figure S5). FC-72 was used as the working fluid in this system. The evaporator was made of an aluminum tube with the inner diameter (ID) of 6mm, the outer diameter (OD) of 8mm, and the length of 200 cm. The experiments were performed at four different chamber temperatures. Inside the chamber, an electrical heater fan (2000W) connected to a PID (Proportional Integral Derivative) controller keeps the chamber temperature at a desired constant value. While the electrical heater heats up the chamber, the coolant passing through the evaporator cools down the hot air. A power-meter device was used to obtain the power consumptions. The power consumption of the electrical heater in the chamber was measured for cases of non-coated surface and bio-coated evaporators.

For the air conditioning system, the energy efficiencies of the bio-coated evaporators were investigated by comparing the power consumption of the electrical heaters for bio-coated and non-coated surface evaporators. Each test lasted for an hour, and the average of power consumption was eventually calculated for each sample. The experiments were performed at four different chamber temperatures of 56.5℃, 58.5℃, 61℃ and 66℃ temperatures (corresponding to 0.5K, 2.5K, 5K and 10K wall superheats, respectively). While the chamber temperature was raised by the heater fan, the evaporator reduced its temperature by absorbing the chamber heat. The PID system deactivated and activated the heater when the temperature of the chamber was higher and lower than the regulated temperature, respectively

Figure 6b shows the obtained results for the bio-coated and non-coated surface evaporators under experimental conditions. The obtained results indicate that the modified evaporators have higher cooling capacities compared to the non-coated surface specimen. Here, the cooling power is the amount of absorbed heat to keep the chamber at the desired constant temperatures. The wall

superheat in the miniature evaporator is defined as the temperature difference between the chamber temperature and the temperature of the fluid before entering the evaporator. On the other hand, the pressure drops for different components of the setup were obtained and compared. Accordingly, the obtained pressure drops for bio-coated evaporators are almost the same as for the non-coated surface evaporator (only ~3% higher). Coefficient of Performance (COP) was used to evaluate the performance of the system. COP was calculated as:

$$COP_{cooling} = \frac{Q_c}{W} \tag{6}$$

In Equation 6, Q_c is the heat removed from the heat source (electrical fan) and W is the consumed work by the system. The consumed work is the sum of pumping power, preheater power and chiller power. Related information about the energy consumption of the system components is given in Supporting Information. Compared to the Non-coated evaporator, the porous-coated evaporator results in enhancements of 0.41%, 1.15%, 6.33% and 11.11%, while the rough-coated evaporator leads to enhancements of 1.66%, 4.38%, 4.66% and 4.44% in cooling COP for chamber at air temperatures of 56.5℃, 58.5℃, 61℃ and 66℃, respectively. The obtained results imply a considerable reduction in energy consumption for thermal-fluids applications.

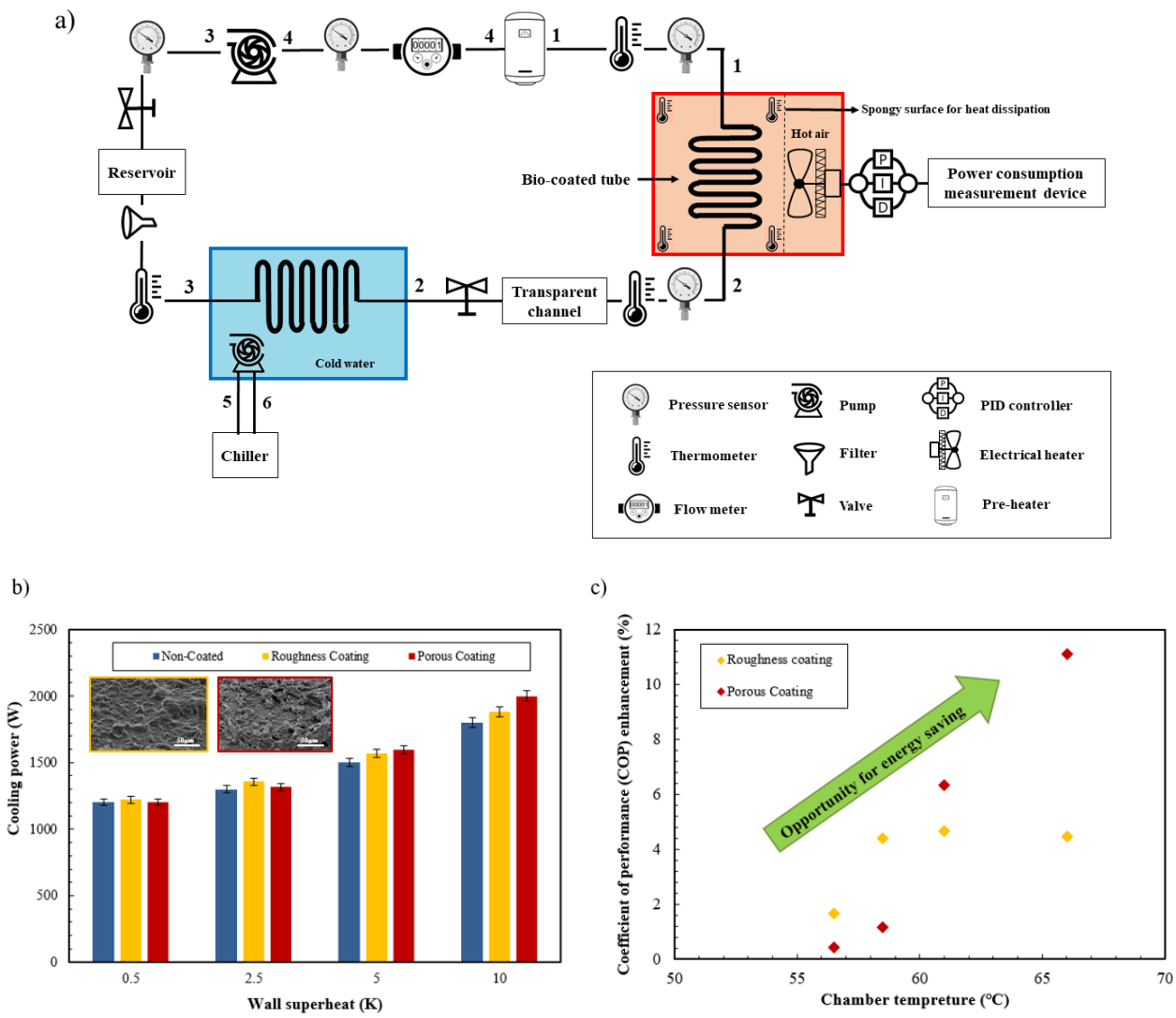

Figure 6. a) Schematic of the lab-made miniature air conditioning system**. b)** Obtained cooling power for bio-coated and non-coated surface evaporators at different wall superheats and the SEM images of the bio-coated aluminum surfaces. **c)** Obtained enhancements in COP for the rough and porous coatings at different chamber temperatures

According to the obtained results, it can be concluded that the proposed coating has the potential to be used in different applications. Rough-coated refrigerator shows higher enhancement at low wall superheats ($\Delta T<2.5K$) compared to porous-coating, which agrees with the obtained results from fundamental studies. This kind of coating is suitable for small-scale refrigerators with low cooling capacities. On the other hand, porous coating offering a superior COP enhancement at medium and high wall superheats is suitable for larger refrigerators with high cooling capacities.

3.5. Exergy analysis, second law

In this section, the second law analysis is presented to give more insight into the energy recovery (exergy availability) for non-coated and coated evaporators. The following expression can be written based on the general exergy balance [46]:

$$\dot{E}_{dest} = \dot{E}_{in} - \dot{E}_{out} = \dot{m}(e_{in} - e_{out}) \tag{7}$$

where $\dot{E}_{in}$ and $\dot{E}_{out}$ are the total exergy (transferred by heat, work and mass) at the inlet and outlet, respectively, and $\dot{E}_{dest}$ is the rate of exergy destruction. For the ambient temperature of T_0 and assuming that the change in kinetic and potential energies is negligible, the exergy is given as:

$$e = (h - h_0) - T_0(S - S_0) \tag{8}$$

The component-wise analysis for the air conditioning system including evaporator, condenser, preheater and pump are as follows:

- Evaporator:

$$\dot{E}_{dest,ev} = \left(\dot{E}_1 - \dot{E}_2\right) + \dot{Q}_c\left(1 - \frac{T_0}{T_L}\right) = \dot{m}(h_1 - T_0S_1) - \dot{m}(h_2 - T_0S_2) + \dot{Q}_L\left(1 - \frac{T_0}{T_L}\right) \tag{9}$$

- Condenser:

$$\dot{E}_{dest,cond} = \left(\dot{E}_2 - \dot{E}_3\right) + \left(\dot{E}_5 - \dot{E}_6\right) \tag{10}$$

$$= \dot{m}(h_2 - T_0S_2) - \dot{m}(h_3 - T_0S_3) + \dot{m}(h_5 - T_0S_5) - \dot{m}(h_6 - T_0S_6)$$

- Pump:

$$\dot{W}_{pump} = \dot{m}(h_3 - h_4) \tag{11}$$

$$\dot{E}_{dest,pump} = \left(\dot{E}_3 - \dot{E}_4\right) + \dot{W}_{pump} = \dot{m}(T_0(S_4 - S_3)) \tag{12}$$

- Preheater:

$$\dot{E}_{dest,pre} = \left(\dot{E}_1 - \dot{E}_4\right) = \dot{m}(h_1 - T_0S_1) - \dot{m}(h_4 - T_0S_4) \tag{13}$$

- Total:

$$\dot{E}_{dest,tot} = \dot{E}_{dest,ev} + \dot{E}_{dest,cond} + \dot{E}_{dest,pump} + \dot{E}_{dest,pre} \quad (14)$$

Exergy destruction permits the evaluation of exergy destroyed per component. The quality of the vapor was obtained using a transparent channel at the outlet of the evaporator, and the images was post-processed using ImageJ software. FC-72, with given properties in Table 2, was used as the working fluid in the closed-loop system.

Table 2. FC-72 properties

Saturation temperature (K)	Liquid density (kg/m^3)	Vapor density (kg/m^3)	Liquid enthalpy (kJ/kg)	Vapor enthalpy (kJ/kg)	Liquid Entropy (KJ/kg.K)	Vapor Entropy (KJ/kg.K)
296	1724.8	3.88	58.48	163.78	0.218	0.563
329	1601.55	13.07	94.76	189.81	0.334	0.616
330	1597.8	13.49	95.88	190.82	0.338	0.619

The first law analysis highlights that the rough- and porous-coated evaporators work more efficiently at low and high temperatures, respectively. Thus, the exergy analysis was performed on rough- and porous-coated surface at wall superheats of 0.5 K and 5 K, respectively. Vapor qualities, cooling powers, COPs and evaporator exergy destruction rates are tabulated in Table 3.

Table 3. Conditions of the exergy analysis

Wall superheat (K)	Evaporator type	Vapor Quality(x)	Cooling power (W)	Coefficient of Performance (enhancement)	Evaporator Exergy destruction (W) (enhancement)
0.5	Non-coated	0	1195	3.428	21.53
	Rough coated	0.07	1220	3.485 (1.6%)	19.91 (7.5%)
5	Non-coated	0.38	1505	4.285	14.15
	Porous coated	0.47	1595	4.557 (6.6%)	12.98 (8.2%)

Figure 7a and 7b illustrate the pressure-enthalpy diagrams for the low and high wall superheat experiments, respectively. Under the experimental conditions it can be observed that the rough-

coated evaporator enhances the exergy destruction ratio up to 7.5% compared to the non-coated case (as shown in Figure 7c). On the other hand, the porous-coated evaporator demonstrates a 8.2% decrease in the exergy destruction ratio compared to the non-coated case (Figure7d).

The second Law analysis is an additional approach for the analysis of heat exchanging devices and allows to evaluate the energy flow between the evaporator surface and the coolant, combining heat transfer and friction effects. Exergy destruction in flow boiling strongly depends on the distribution of vapor and liquid phases inside the evaporator. Since the bio-coating thicknesses are negligible compared to the tube diameter, the frictional pressure drop in two-phase flows can be considered as the main source of exergy destruction.

The larger exergy losses between evaporator inlet and outlet in the non-coated evaporator are due to i) higher wall superheats required for the onset of nucleate boiling, ii) non-uniform surface temperature due to lower number of active nucleation sites, iii) larger frictional pressure drop due to the presence of larger vapor bubbles [47],[48],[49]. Generated larger bubbles (Figure 5) on the non-coated evaporator results in larger bubble slip velocity and higher deformability, which all eventually increase the frictional pressure drop of the boiling flow inside the 2-m long evaporator [50].

By improving the phase change process, the coated specimens generate more vapors inside the evaporator. Therefore, the inlet vapor quality of the condenser is higher for the coated evaporator compared to the non-coated one. As a result, the exergy destruction rate for the condenser is higher for the cycles that utilize enhanced evaporators.

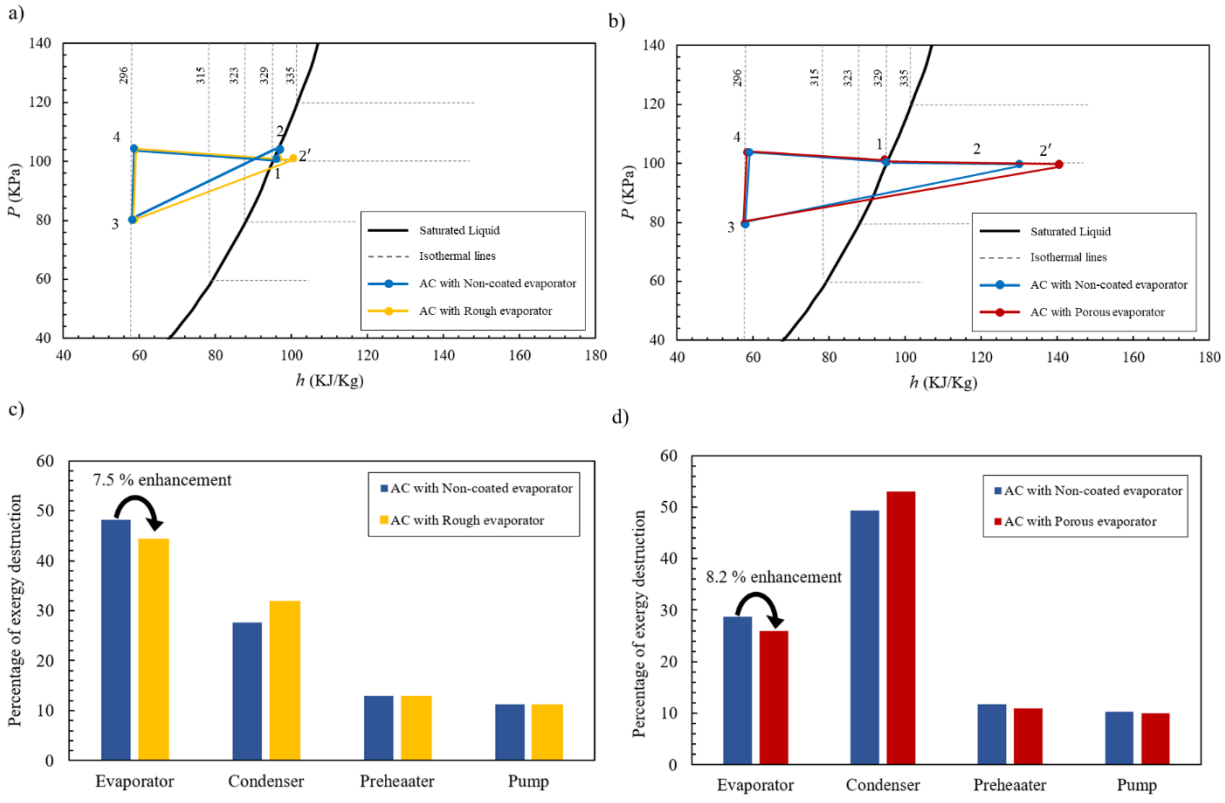

Figure 7. a,b) Thermodynamic cycle of two phase air conditioning system with rough- and porous- and non-coated evaporators. Here, the rough-coated evaporator is tested and compared to the non-coated evaporator at wall superheat of 0.5 K and porous-coated evaporator was tested and compared to the non-coated evaporator at wall superheat of 5 K. c,d) Percentage of exergy destruction in different components of the lab-made air conditioning system with the mentioned evaporators

Air conditioning systems - most important energy systems - are one of the largest energy consumers in residential and commercial buildings. In the United States alone 400 terawatt-hours of electricity are consumed annually for air conditioning purposes [51]. Setting higher efficiency standards for cooling devices is one of the approaches, which can dramatically reduce the need for new power plants, cut gas emissions, and reduce the costs. Our proposed bio-coating to be implemented to air conditioning systems will not only significantly reduce the green-house gas emission but it will also assist in saving billions of dollars.

4. Conclusion

A new class of bio-based surface modification technique for thermal-fluid applications is presented and validated using a heat resistant microorganism; *Sulfolobus solfataricus*. The proposed bio-coating was cultured and optimized to provide organic roughness and porous coating on the desired metallic and non-metallic substrates. Fundamental studies were performed to investigate the enhancement in boiling heat transfer. Afterwards, the coating was successfully adapted and tested in miniature air-conditioning systems for performance assessment. Significant enhancements in performances (based on both first and second laws of thermodynamics) were achieved. Unlike most of the available surface modification techniques, which require expensive microfabrication devices (physical modifications) and have damaging impact on the environment (chemical modifications), the proposed technique is economical, scalable, biocompatible and eco-friendly.

Supporting Information

Coating apparatus, boiling and air conditioning experimental setups, data reduction and uncertainty analysis are provided in the Supporting Information file.

Author Contributions

S.N. and A.K.S. designed the experimental setups and conducted the experiments. V.O.K. and G.G prepared and optimized the bio-mixture. S.Ç. characterized the samples. G.G, Ö.K and A.K. provided guidance and comments. A.K.S and A.K. supervised the project. All the authors contributed to the preparation of the manuscript.

Declaration of Interests

The authors declare no competing interests.

Acknowledgements

This study was supported by TUBITAK (The Scientific and Technological Research Council of Turkey) Support Program for Scientific and Technological Research Project Grant No.

119C026. The equipment and characterization supports are provided by the Sabanci University Nanotechnology Research and Applications Center (SUNUM). The authors also thank Mohammad Jafarpour and Kosar Hassannezhad for their assistance in capturing Scanning Electron Microscopy (SEM) images.

References

[1] International energy agency (IEA), n.d. https://www.iea.org/news/air-conditioning-use-emerges-as-one-of-the-key-drivers-of-global-electricity-demand-growth (accessed September 2, 2020).
[2] Mudawar I. Assessment of high-heat-flux thermal management schemes. IEEE Trans Components Packag Technol 2001;24:122–41.
[3] Thome JR. Boiling in microchannels: a review of experiment and theory. Int J Heat Fluid Flow 2004;25:128–39.
[4] Xie S, Beni MS, Cai J, Zhao J. Review of critical-heat-flux enhancement methods. Int J Heat Mass Transf 2018;122:275–89.
[5] Attinger D, Frankiewicz C, Betz AR, Schutzius TM, Ganguly R, Das A, et al. Surface engineering for phase change heat transfer: A review. MRS Energy Sustain 2014;1.
[6] Shojaeian M, Koşar A. Pool boiling and flow boiling on micro-and nanostructured surfaces. Exp Therm Fluid Sci 2015;63:45–73.
[7] Yao Z, Lu Y-W, Kandlikar SG. Effects of nanowire height on pool boiling performance of water on silicon chips. Int J Therm Sci 2011;50:2084–90.
[8] Demir E, Izci T, Alagoz AS, Karabacak T, Koşar A. Effect of silicon nanorod length on horizontal nanostructured plates in pool boiling heat transfer with water. Int J Therm Sci 2014;82:111–21.
[9] Sadaghiani AK, Motezakker AR, Kasap S, Kaya II, Koşar A. Foamlike 3D graphene coatings for cooling systems involving phase change. ACS Omega 2018;3:2804–11.
[10] Khalili Sadaghiani A, Reza Motezakker A, Volkan Özpınar A, Özaydın İnce G, Koşar A. Pool boiling heat transfer characteristics of inclined pHEMA-coated surfaces. J Heat Transfer 2017;139.
[11] Çıkım T, Armağan E, Ozaydin Ince G, Koşar A. Flow Boiling Enhancement in Microtubes With Crosslinked pHEMA Coatings and the Effect of Coating Thickness. J Heat Transfer 2014;136. https://doi.org/10.1115/1.4027352.
[12] Rahman MM, Ölçeroğlu E, McCarthy M. Scalable Nanomanufacturing of Virus-templated Coatings for Enhanced Boiling. Adv Mater Interfaces 2014;1:1300107.
[13] Motezakker AR, Sadaghiani AK, Çelik S, Larsen T, Villanueva LG, Koşar A. Optimum ratio of hydrophobic to hydrophilic areas of biphilic surfaces in thermal fluid systems involving boiling. Int J Heat Mass Transf 2019;135:164–74.
[14] Patil CM, Kandlikar SG. Review of the manufacturing techniques for porous surfaces used in enhanced pool boiling. Heat Transf Eng 2014;35:887–902.
[15] Može M, Senegačnik M, Gregorčič P, Hočevar M, Zupančič M, Golobič I. Laser-Engineered Microcavity Surfaces with a Nanoscale Superhydrophobic Coating for Extreme Boiling Performance. ACS Appl Mater Interfaces 2020;12:24419–31.
[16] Bostanci H, Singh V, Kizito JP, Rini DP, Seal S, Chow LC. Microscale surface

modifications for heat transfer enhancement. ACS Appl Mater Interfaces 2013;5:9572–8.
[17] Ma A, Wei J, Yuan M, Fang J. Enhanced flow boiling heat transfer of FC-72 on micro-pin-finned surfaces. Int J Heat Mass Transf 2009;52:2925–31.
[18] Sadaghiani AK, Saadi NS, Parapari SS, Karabacak T, Keskinoz M, Koşar A. Boiling heat transfer performance enhancement using micro and nano structured surfaces for high heat flux electronics cooling systems. Appl Therm Eng 2017;127:484–98.
[19] Alam T, Lee PS, Yap CR. Effects of surface roughness on flow boiling in silicon microgap heat sinks. Int J Heat Mass Transf 2013;64:28–41.
[20] Jung J-Y, Kwak H-Y. Effect of surface condition on boiling heat transfer from silicon chip with submicron-scale roughness. Int J Heat Mass Transf 2006;49:4543–51.
[21] Şişman Y, Sadaghiani AK, Khedir KR, Brozak M, Karabacak T, Koşar A. Subcooled flow boiling over microstructured plates in rectangular minichannels. Nanoscale Microscale Thermophys Eng 2016;20:173–90.
[22] Rainey KN, Li G, You SM. Flow boiling heat transfer from plain and microporous coated surfaces in subcooled FC-72. J Heat Transf 2001;123:918–25.
[23] Sarwar MS, Jeong YH, Chang SH. Subcooled flow boiling CHF enhancement with porous surface coatings. Int J Heat Mass Transf 2007;50:3649–57.
[24] Zhao CY, Lu W, Tassou SA. Flow boiling heat transfer in horizontal metal-foam tubes. J Heat Transfer 2009;131.
[25] Pranoto I, Leong KC. An experimental study of flow boiling heat transfer from porous foam structures in a channel. Appl Therm Eng 2014;70:100–14.
[26] Paints and Coatings Market Size, Trends, Share, Report 2027. n.d. https://www.fortunebusinessinsights.com (accessed August 28, 2020).
[27] Motezakker AR, Sadaghiani AK, Akkoc Y, Parapari SS, Gözüaçık D, Koşar A. Surface modifications for phase change cooling applications via crenarchaeon Sulfolobus solfataricus P2 bio-coatings. Sci Rep 2017;7:1–9.
[28] Ciaramella M, Pisani FM, Rossi M. Molecular biology of extremophiles: recent progress on the hyperthermophilic archaeon Sulfolobus. Antonie Van Leeuwenhoek 2002;81:85–97.
[29] Chaban B, Ng SYM, Jarrell KF. Archaeal habitats—from the extreme to the ordinary. Can J Microbiol 2006;52:73–116.
[30] Schleper C, Puehler G, Holz I, Gambacorta A, Janekovic D, Santarius UTE, et al. Picrophilus gen. nov., fam. nov.: a novel aerobic, heterotrophic, thermoacidophilic genus and family comprising archaea capable of growth around pH 0. J Bacteriol 1995;177:7050–9.
[31] Kashefi K, Lovley DR. Extending the Upper Temperature Limit for Life. Science (80-) 2003;301:934 LP – 934. https://doi.org/10.1126/science.1086823.
[32] Grogan DW. Phenotypic characterization of the archaebacterial genus Sulfolobus: comparison of five wild-type strains. J Bacteriol 1989;171:6710 LP – 6719. https://doi.org/10.1128/jb.171.12.6710-6719.1989.
[33] Ohki S, Arnold KBT-M in E. Determination of Liposome Surface Dielectric Constant and Hydrophobicity. Liposomes, Part A, vol. 367, Academic Press; 2003, p. 253–72. https://doi.org/https://doi.org/10.1016/S0076-6879(03)67016-3.
[34] Allocati N, Masulli M, Di Ilio C, De Laurenzi V. Die for the community: an overview of programmed cell death in bacteria. Cell Death Dis 2015;6:e1609–e1609.
[35] Simon G, Walther J, Zabeti N, Combet-Blanc Y, Auria R, Van Der Oost J, et al. Effect of O2 concentrations on Sulfolobus solfataricus P2. FEMS Microbiol Lett 2009;299:255–60.

[36] Ulas T, Riemer SA, Zaparty M, Siebers B, Schomburg D. Genome-scale reconstruction and analysis of the metabolic network in the hyperthermophilic archaeon Sulfolobus solfataricus. PLoS One 2012;7:e43401.
[37] Clarke PH. Hydrogen sulphide production by bacteria. Microbiology 1953;8:397–407.
[38] Jørgensen BB. Mineralization of organic matter in the sea bed—the role of sulphate reduction. Nature 1982;296:643–5.
[39] Luther GW, Findlay AJ, MacDonald DJ, Owings SM, Hanson TE, Beinart RA, et al. Thermodynamics and kinetics of sulfide oxidation by oxygen: a look at inorganically controlled reactions and biologically mediated processes in the environment. Front Microbiol 2011;2:62.
[40] Canfield DE, Thamdrup B. The production of 34S-depleted sulfide during bacterial disproportionation of elemental sulfur. Science (80-) 1994;266:1973–5.
[41] Chen X, Andersen TJ, Morono Y, Inagaki F, Jørgensen BB, Lever MA. Bioturbation as a key driver behind the dominance of Bacteria over Archaea in near-surface sediment. Sci Rep 2017;7:1–14.
[42] Chen X, Wang X, Chen PG, Liu Q. Determination of diffusion coefficient in droplet evaporation experiment using response surface method. Microgravity Sci Technol 2018;30:675–82.
[43] Solubility of Gases in Water n.d. https://www.engineeringtoolbox.com (accessed September 2, 2020).
[44] McQuiston FC, Parker JD, Spitler JD. Heating, ventilating, and air conditioning: analysis and design. John Wiley & Sons; 2004.
[45] Sadaghiani AK, Altay R, Noh H, Kwak HJ, Şendur K, Mısırlıoğlu B, et al. Effects of bubble coalescence on pool boiling heat transfer and critical heat flux–A parametric study based on artificial cavity geometry and surface wettability. Int J Heat Mass Transf 2020;147:118952.
[46] Dincer I, Kanoglu M. Refrigeration systems and applications. vol. 2. Wiley Online Library; 2010.
[47] Chávez CA, Leão HLSL, Ribatski G. Evaluation of thermal-hydraulic performance of hydrocarbon refrigerants during flow boiling in a microchannels array heat sink. Appl Therm Eng 2017;111:703–17.
[48] Yang M-H, Yeh R-H. Performance and exergy destruction analyses of optimal subcooling for vapor-compression refrigeration systems. Int J Heat Mass Transf 2015;87:1–10.
[49] Karimzadehkhouei M, Shojaeian M, Sadaghiani AK, Şendur K, Mengüç MP, Koşar A. Entropy generation analysis of laminar flows of water-based nanofluids in horizontal minitubes under constant heat flux conditions. Entropy 2018;20:242.
[50] Murai Y. Frictional drag reduction by bubble injection. Exp Fluids 2014;55:1773.
[51] Biardeau LT, Davis LW, Gertler P, Wolfram C. Heat exposure and global air conditioning. Nat Sustain 2020;3:25–8.

Supporting Information

Bio-coated surfaces with micro-roughness and micro-porosity: Next generation coatings for enhanced energy efficiency

Soroush Niazi[1,2], *Abdolali K Sadaghiani*[1,2,*], *Veysel Ogulcan Kaya*[1,2], *Ghazaleh Gharib* [1,2], *Süleyman Çelik*[1], *Özlem Kutlu*[1,2], *Ali Kosar*[1,2,3,*]

[1]Sabanci University Nanotechnology Research and Application Center, 34956 Tuzla, Istanbul, Turkey

[2]Faculty of Engineering and Natural Science, Sabanci University, 34956 Tuzla, Istanbul, Turkey

[3]Center of Excellence for Functional Surfaces and Interfaces for Nano-Diagnostics (EFSUN), Sabanci University, Orhanli, 34956, Tuzla, Istanbul, Turkey

[*] Corresponding authors; E-mail: kosara@sabanciuniv.edu, abdolali@sabanciuniv.edu

Supporting Information

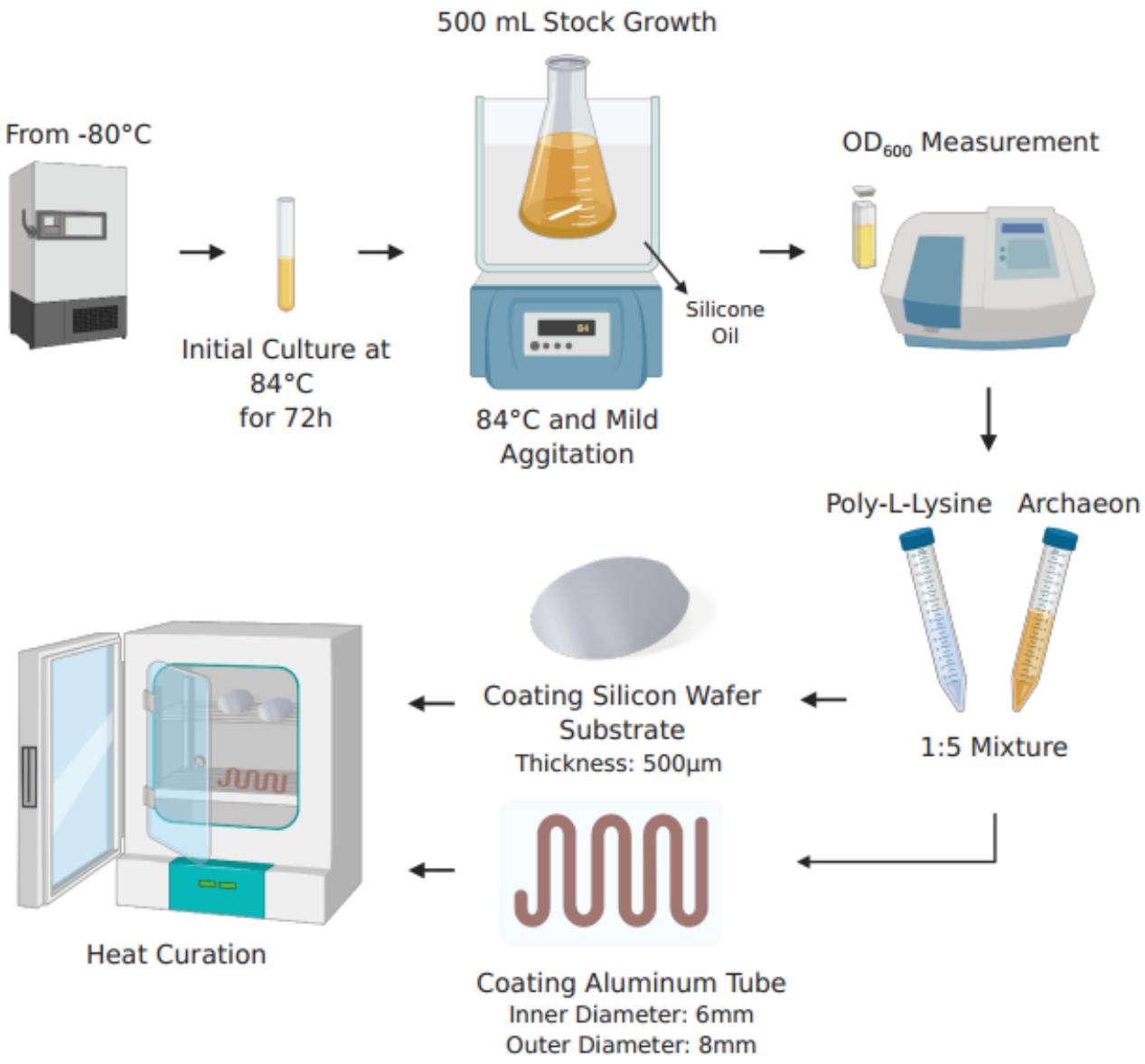

Figure S1. Culturing, coating and drying processes of *Sulfolobus Solfataricus.*

Supporting Information

Table S1. *Sulfoloubus solfactricus* Medium compositions

ATCC medium (1304 *Sulfoloubus solfactricus* medium)	**Amount**
Yeast Extract (BD 212750)	1 g
Casamino Acids (BD 223050)	1 g
KH_2PO_4	3.1 g
$(NH_4)_2\ SO_4$	2.5 g
$MgSO_4$. 7 H_2O	0.2 g
$CaCl_2$. 2 H_2O	0.25 g
$MnCl_2$. 4 H_2O	1.8 mg
$Na_2B_4O_7$. 10 H_2O	4.5 mg
$ZnSO_4$. 7 H_2O	0.22 mg
$CuCl_2$. 2 H_2O	0.05 mg
Na_2MoO_4 . 2 H_2O	0.03 mg
$VOSO_4$. 2 H_2O	0.03 mg
$CoSO_4$. 7 H_2O	0.01 mg
Distilled water	1 L

Supporting Information

Coating process of the aluminum tube

A lab-made long oven was prepared to dry the coated long tube while rotating. The drying system is shown in Figure S2. The air was blown by air compressor to the heat chamber and the temperature of the air was increased to 300℃. The heating part has a resistance in a lamp, which acquires power from the power supply. It passes into five paths to dry the pipe in five regions of the oven. The pipe has 6 ball bearings to keep the pipe straight during the rotation. The inner volume of this 2 meter long tube is about 60 ml and the archaea's mixture volume injected to the tube is about 40 ml to allow the fluid to evaporate better during the rotation. After being sure that the inside of the tube was coated and it was dry, the 2 meter long tube was bent by the Swagelok tube bender to make the evaporator.

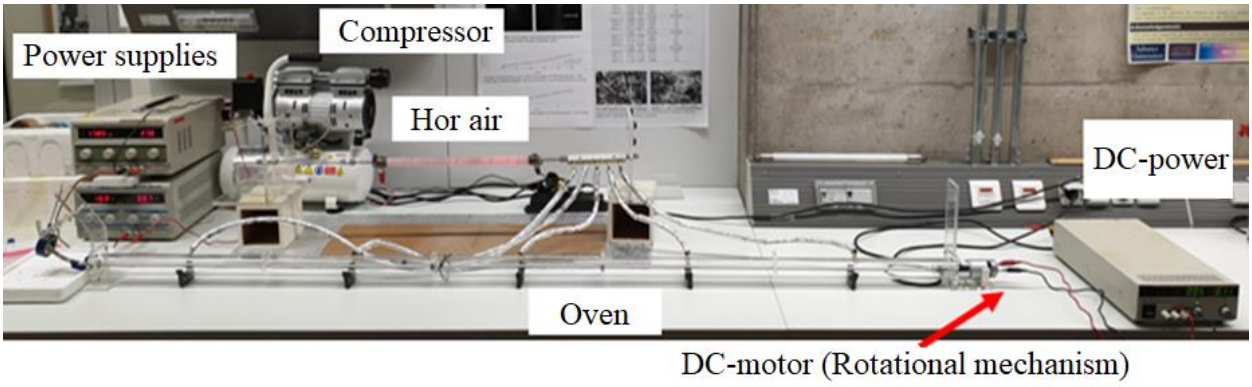

Figure S2. The coating system for the aluminum tube

Supporting Information

Metallic bio-coated surfaces

SEM (Scanning Electron Microscopy) images of the bio-coatings on top of the metallic substrates such as stainless steel, aluminum and copper are depicted in Figure S3.

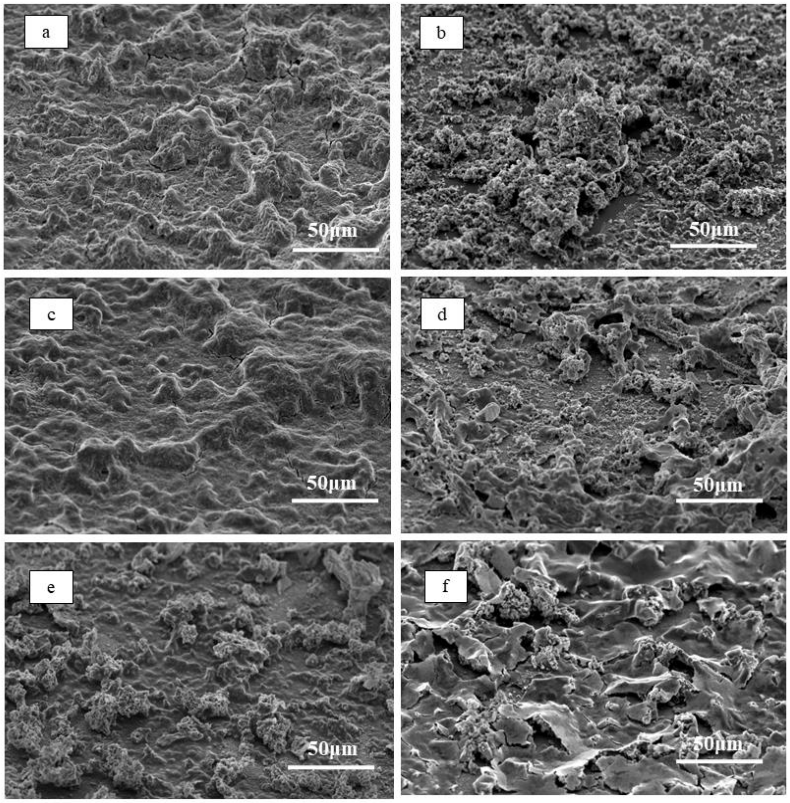

Figure S3. SEM images of the surface morphologies on different metallic substrates: **a)** roughness coating on stainless steel, **b)** porous coating on stainless steel, **c)** roughness coating on aluminum, **d)** porous coating on aluminum, **e)** roughness coating on copper, **f)** porous coating on copper

Supporting Information

Boiling test section

The schematic of the boiling setup is demonstrated in Figure S4. Two cartridge heaters were used for applying heat from the bottom of the channel. A digital power supply was connected to cartridge heaters, and current and voltage were measured at every heat flux. The test section was made of aluminum. To minimize the heat losses, Teflon was used surrounding the aluminum block. A plexiglass was utilized on top of the channel, which allow the flow visualization from the top. Two holder plates were used on top and bottom of the setup to sandwich the Plexiglass on top of plastic O-rings. A commercial camera, Canon EOS 70D, was used to visualize boiling during heating. Four horizontal holes were formed in the aluminum block under the surface of the minichannel to measure the surface temperatures using T-type thermocouples and UNI-T UT325 Contact thermometers. The bio-coated silicon was located on top of the aluminum block. Deepcool Z3 paste, a superconductive thermal paste, was used for attaching the silicon surface on the aluminum block. A micro gear pump was used to pump the fluid through the system. Deionized water was used as the working fluid. The working fluid was degassed using a vacuum tank to remove dissolved gas from the water by lowering the pressure inside the tank and was then introduced into the preheater section before entering the boiling test section. The preheater was an immersed heat exchanger in 100℃ silicon oil whose temperature was controlled with a PID controller.

Supporting Information

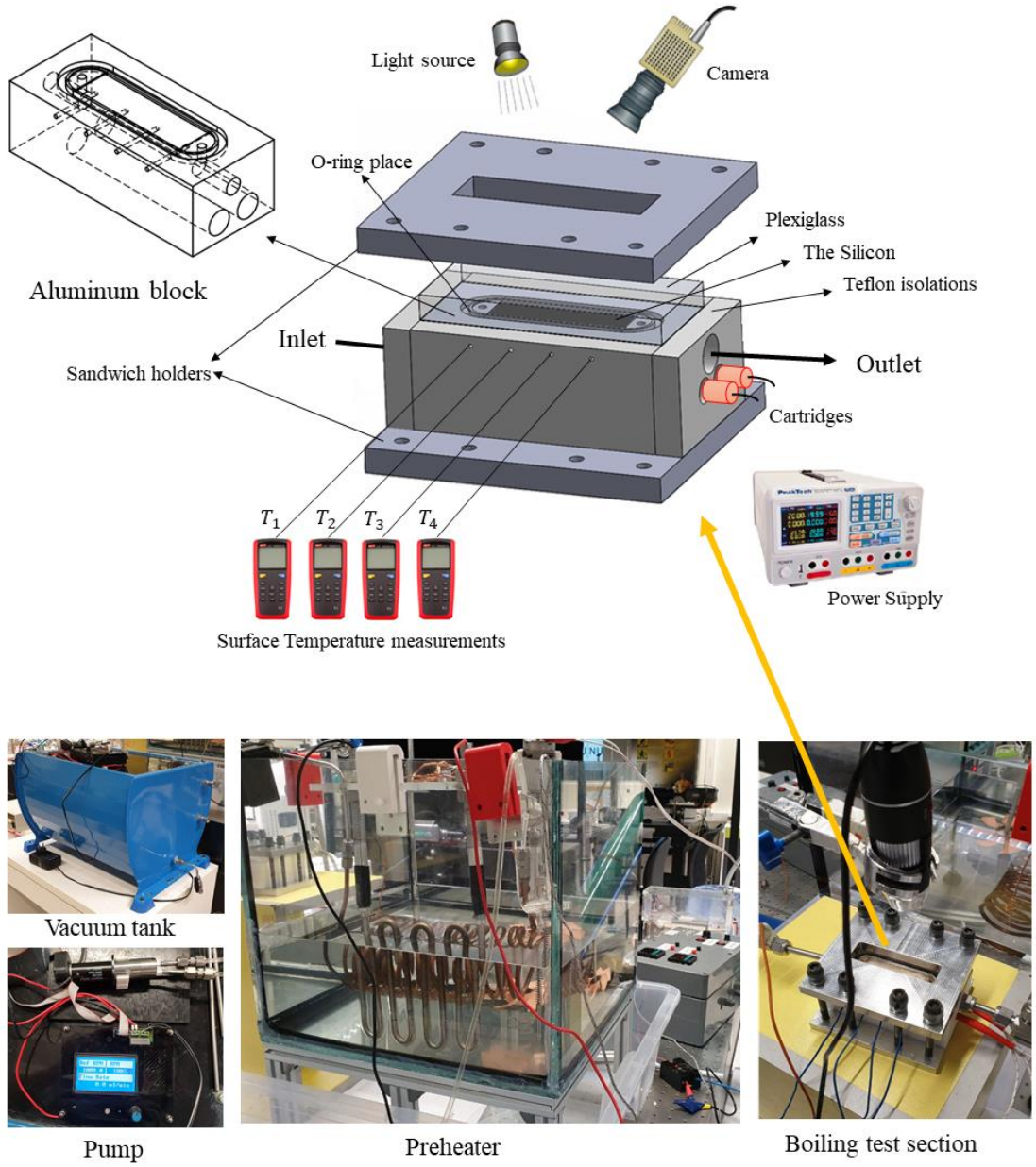

Figure S4. Open loop boiling test section

Supporting Information

Lab-made close-loop air condition system

Figure S5 depicts the experimental setup of the miniature air conditioning system, which was assembled to measure the cooling performance of the bio-coated aluminum tube. It consists of a condenser, a chiller, a pump, a preheater, a reservoir, valves, and the test section. The temperatures and pressures at different locations were measured using UNI-T UT325 thermometers connected to T-type thermocouples and pressure gauge (Omega). A preheater is placed before the test section to keep the inlet temperature of the coolant at 56°C. Two thermocouples were installed for temperature measurement, one prior to entering the evaporator and the other one at the exit of the evaporator. The test section was a constant temperature chamber, which includes an electrical heater, four thermocouples for air temperature measurements, two thermocouples for coolant temperature measurements, a fan, a spongy pad for heat dissipation and the evaporator. The chamber walls were thermally isolated via 5 mm thick ceramic paper to reduce the thermal losses.

The consumed work by the system is the sum of pumping power, preheater power and the chiller power. The pumping power kept constant at 10.2 W for pumping the fluid at flow rate of 1.66 ml/s and mass flux of 100 kg/m^{2}s. The preheater connected to a power supply consumed 110W to increase the fluid's temperature from 23℃ to 56℃. The condenser connected to a chiller use 220W to reduce the temperature of the heated fluid to 23℃.

Supporting Information

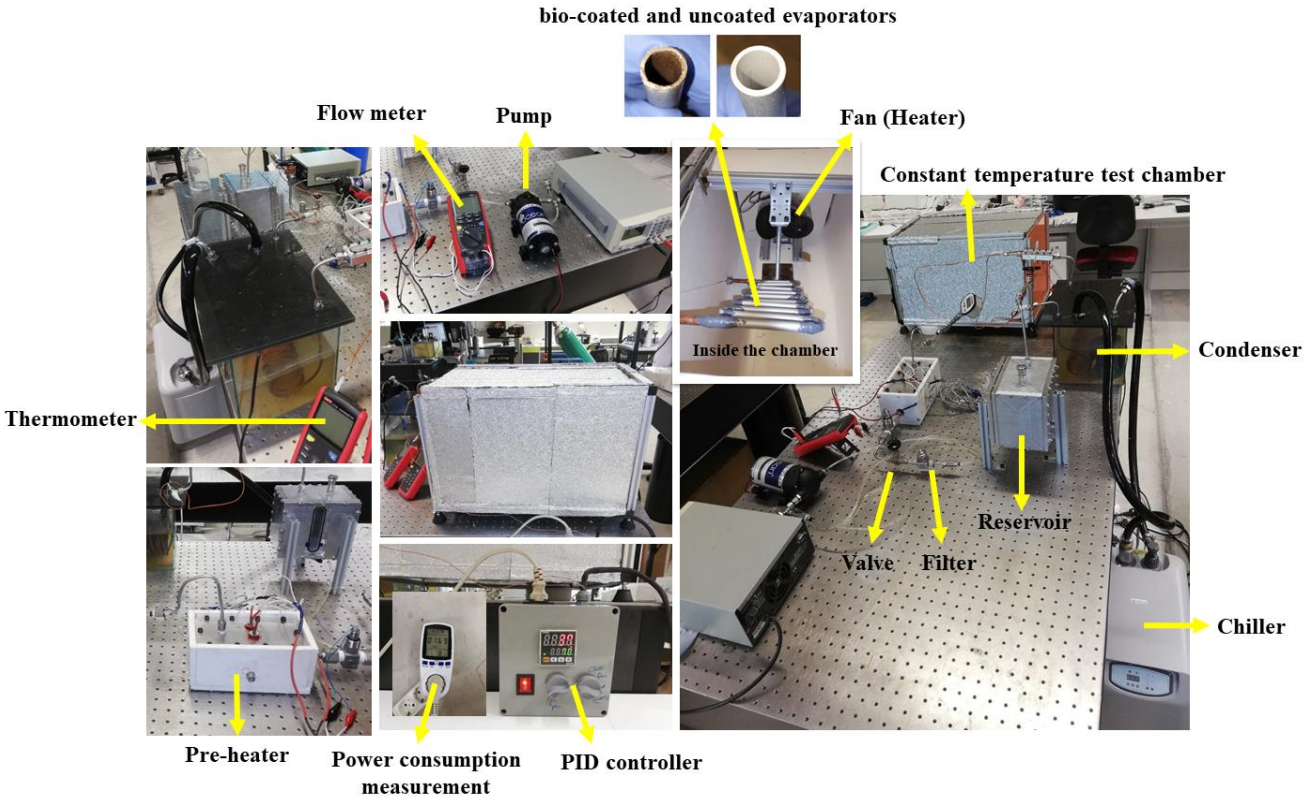

Figure S5. Experimental setup of the lab-made miniature air conditioning system

Supporting Information

Uncertainty analysis

Uncertainty analysis was based on the error propagation of experimental data using the methodology proposed by Coleman et al. [1]. The general formulation is expressed as:

$$U_y = \sqrt{\sum_{i=1}^{n} \left\{ \left(\frac{\partial y}{\partial x_i} \right) . U_{x_i} \right\}^2}$$

U_{x_i} is the uncertainty in parameter x_i. The parameters in our experiments with the corresponding uncertainties are listed in Table S2.

Table S2: Uncertainties in parameters

Parameters	Uncertainties
Voltage	±1 V
Current	± 0.1 A
Thermocouples	±0.5 ℃
Heat flux	±5%
Flow meter	±2%
Pressure	±5%
Heat transfer coefficient	±3%
Coefficient of performance	±3%

References

[1] Coleman HW, Steele WG. Experimentation, validation, and uncertainty analysis for engineers. John Wiley & Sons; 2018.